

# Vib2ECG: A Paired Chest-Lead SCG–ECG Dataset and Benchmark for ECG Reconstruction

Guorui Lu, *Student Member, IEEE*, Xiaohui Cai,  
Todor Stefanov, *Member, IEEE*, Qinyu Chen, *Member, IEEE*

**Abstract**—Twelve-lead electrocardiography (ECG) is essential for cardiovascular diagnosis, but its long-term acquisition in daily life is constrained by complex and costly hardware. Recent efforts have explored reconstructing ECG from low-cost cardiac vibrational signals such as seismocardiography (SCG), however, due to the lack of a dataset, current methods are limited to limb leads, while clinical diagnosis requires multi-lead ECG, including chest leads. In this work, we propose Vib2ECG, the first paired, multi-channel electro-mechanical cardiac signal dataset<sup>1</sup>, which includes complete twelve-lead ECGs and vibrational signals acquired by inertial measurement units (IMUs) at six chest-lead positions from 17 subjects. Based on this dataset, we also provide a benchmark. Experimental results demonstrate the feasibility of reconstructing electrical cardiac signals at variable locations from vibrational signals using a lightweight 364 K-parameter U-Net. Furthermore, we observe a hallucination phenomenon in the model, where ECG waveforms are generated in regions where no corresponding electrical activity is present. We analyze the causes of this phenomenon and propose potential directions for mitigation. This study demonstrates the feasibility of mobile-device-friendly ECG monitoring through chest-lead ECG prediction from low-cost vibrational signals acquired using IMU sensors. It expands the application of cardiac vibrational signals and provides new insights into the spatial relationship between cardiac electrical and mechanical activities with spatial location variation.

**Index Terms**—Dataset, ECG, SCG, ECG Waveform Reconstruction.

## I. INTRODUCTION

ELECTROCARDIOGRAPHY (ECG) is a widely used clinical tool to monitor and diagnose cardiac diseases. In the standard twelve-lead system, there is a mature theoretical framework by which physicians can interpret the ECG waveform and analyze the patient’s condition [1]. However, for chronic cardiovascular diseases that require daily ECG monitoring [2]–[7], wearable ECG devices such as the Holter monitor face challenges. Due to the small amplitude and susceptibility to interference of ECG signals [8], additional

circuitry is required to reduce noise. This both increases the complexity and the costs of ECG devices [9], thereby limiting large-scale use in everyday life. In addition, the complexity of the ECG device circuit also makes its daily use uncomfortable, for example, the device is relatively large and heavy, and multiple electrodes must be attached to the body [10].

Seismocardiography (SCG) is an emerging monitoring tool that uses inertial measurement units (IMUs) or accelerometers to record vibration signals generated by the human heart [11], which contain useful information about cardiac function [12]–[14]. SCG has received increasing attention in recent years, as its cost of sensing hardware continues to decrease as sensor technology advances [15]. Currently, IMUs can cost as little as \$1 [16], whereas ECG devices often cost over \$149 [17]. Moreover, SCG can be acquired using everyday devices such as smartphones [18]–[20] or wristbands [21], [22], which are already equipped with the IMU or accelerometers, further reducing deployment cost and improving accessibility.

However, SCG also has its limitations. Due to the relatively late start of research on SCG [23], the interpretation of SCG waveforms lacks a mature theoretical framework comparable to that of ECG. As a result, SCG signals cannot be directly interpreted by clinicians. Moreover, SCG is easily affected by external factors such as motion [24], [25], which means that although it contains rich information, the signals are difficult to distinguish with the naked eye, further increasing the difficulty of interpretation. Although existing studies have explored the direct application of SCG [26]–[32], they typically focus on a specific disease or parameter estimation and are unable to provide a comprehensive interpretation of the signals comparable to the theoretical framework of ECG.

To overcome the respective limitations of ECG and SCG while combining their complementary strengths, a promising approach is to acquire SCG signals and then convert them into ECG signals. As illustrated in Fig. 1, this strategy retains the low-cost benefit of SCG acquisition, while enabling signal interpretation based on the well-established theoretical framework of ECG [22], [33]–[35]. The physiological motivation behind this approach lies in the electromechanical nature of the heart. The heart functions as an electromechanical pump, in which myocardial contraction is initiated by electrical depolarization [36]. As a result, the heart’s rhythmic mechanical activity occurs under the coordination of electrical signals [37]. These electrical and mechanical processes are therefore tightly coupled and their corresponding signals exhibit correlation. Hence, in theory, it is possible to reconstruct one modality of

Guorui Lu, Todor Stefanov, and Qinyu Chen are with the Leiden Institute of Advanced Computer Science (LIACS), Leiden University, Leiden, The Netherlands. (email: g.lu@liacs.leidenuniv.nl, q.chen@liacs.leidenuniv.nl)

Xiaohui Cai is with the School of Computer Science and Technology, University of Science and Technology of China, Anhui, China.

<sup>1</sup>The dataset can be found in [https://leidenuniv1-my.sharepoint.com/:f/g/personal/lug\\_vuw\\_leidenuniv\\_nl/IgDg5j2CIATlQ56qjY4YIf-vAanPDRScblrc056wRheo7Us?e=KZEeAS](https://leidenuniv1-my.sharepoint.com/:f/g/personal/lug_vuw_leidenuniv_nl/IgDg5j2CIATlQ56qjY4YIf-vAanPDRScblrc056wRheo7Us?e=KZEeAS)

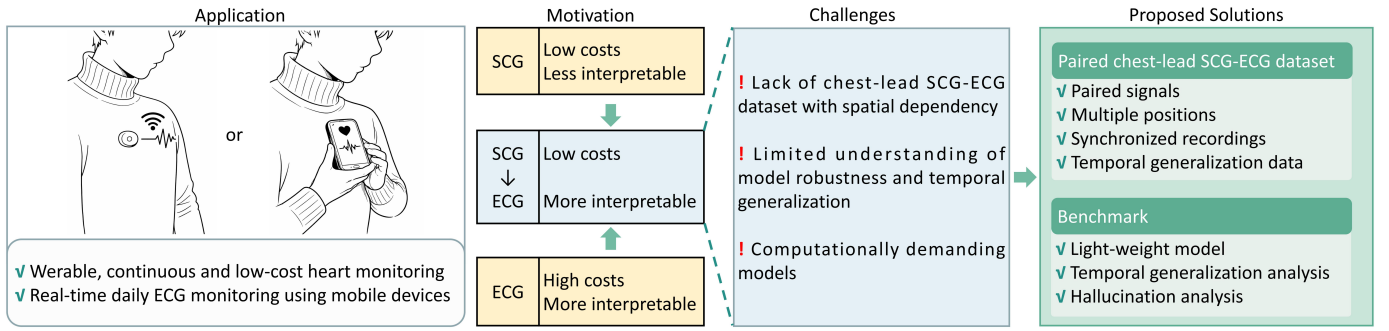


Fig. 1. Conceptual overview of SCG-to-ECG reconstruction for mobile and wearable cardiac monitoring. While SCG offers a cost-effective sensing modality, its limited interpretability motivates the reconstruction of ECG signals. Existing approaches are constrained by the lack of paired chest-lead SCG-ECG datasets. This work addresses these gaps by providing a paired chest-lead dataset based on twelve-lead system and establishing a SCG-to-ECG reconstruction benchmark.

signal from the other.

However, existing SCG-to-ECG conversion methods still have limitations. First, current approaches are restricted to limb-lead ECG reconstruction, whereas the diagnosis of many cardiovascular diseases requires ECG recordings from multiple anatomical locations, particularly chest leads [38]–[40]. Second, in these studies the ECG and SCG signals are collected in an unpaired approach, often from different spatial locations. This mismatch makes it difficult to explore how the relationship between ECG and SCG varies with the change of location. Third, prior methods have not investigated the temporal generalization of learned models over time, leaving their robustness across different time periods largely unexplored.

The primary cause of these limitations is the lack of suitable datasets, which prevents existing methods from addressing spatial and temporal generalization in SCG-to-ECG reconstruction. To fill this gap, we release a paired ECG-SCG dataset collected at chest lead positions from 17 subjects. To the best of our knowledge, this is the first dataset containing multiple locations of paired ECG and SCG signals, and this dataset has the potential for enabling new insights into how the ECG–SCG relation varies by sensor placement. Based on this dataset, we provide a subject-specific benchmark, propose a reconstruction method that decomposes the vibration signals into low-frequency and high-frequency components for joint ECG reconstruction, and offer a physiological and physical explanation. In the process, we identify a “hallucination” phenomenon during ECG reconstruction, in which reconstructed ECG waveforms appear in regions without corresponding electrical activity. We analyze its cause and offer potential directions for mitigation. Finally, to study the temporal generalization of models in this task, we collected data continuously for 8 days from the same subject, exploring how a model trained on the first day performs when tested on subsequent days, thereby preliminarily investigating temporal generalization for SCG-to-ECG reconstruction. In summary, our contributions are as follows:

- We release Vib2ECG, a paired, multi-location chest-lead ECG–SCG dataset, which, to the best of our knowledge, is the first dataset that synchronously records complete twelve-lead ECGs and paired vibrational signals at multiple chest positions.
- Based on the Vib2ECG dataset, we provide a benchmark

model for ECG reconstruction using a subject-specific approach and demonstrate that a lightweight U-Net model (364 K parameters) can reconstruct ECG signals of chest leads with an average L1 distance of 0.1524.

- We systematically identify and analyze a hallucination phenomenon in ECG reconstruction, where fake ECG waveforms are generated without corresponding electrical activity, and investigate its underlying causes.
- We provide a preliminary investigation into temporal generalization by evaluating model performance across multi-day recordings from the same subject. To the best of our knowledge, Vib2ECG is also the first SCG-ECG dataset that includes continuous multi-day recordings from the same subject.

Our ultimate goal is to develop a mobile-deployable system that can predict chest-lead ECG signals using a single smart patch or smartphone placed on the chest. To enable this, the model must learn to infer the corresponding chest-lead ECG solely from the recorded vibrational signal. This makes paired SCG–ECG data at chest-lead locations essential. The present study addresses the lack of such paired data and serves as a first step toward this goal.

## II. RELATED WORK

To leverage both the theoretical foundation of ECG and the low cost of SCG while fully exploiting SCG information, it is feasible to collect SCG signals and convert them into ECG, due to the tight electromechanical coupling of cardiac signals [36]. [33] mounted a geophone on a bed to collect cardiac vibration signals and used a Bi-directional Long Short-Term Memory (Bi-LSTM) to convert them into ECG signals. Physicians were invited to identify the signals, and except for one participant, the rest could not distinguish between real and generated signals. [34] used the CEBS open-source dataset and an attentive cycle-generative adversarial network (CycleGAN) for conversion, achieving a root mean square error (RMSE) of 0.418. [22] collected pulse signals using a wrist-worn accelerometer and converted them into ECG signals with a network combining GAN and encoder-decoder models, achieving a waveform amplitude estimation error of 5.989%. [35] acquired chest vibration signals non-contactly using millimeter-wave radar and performed domain transformation with a transformer-based architecture, obtaining an

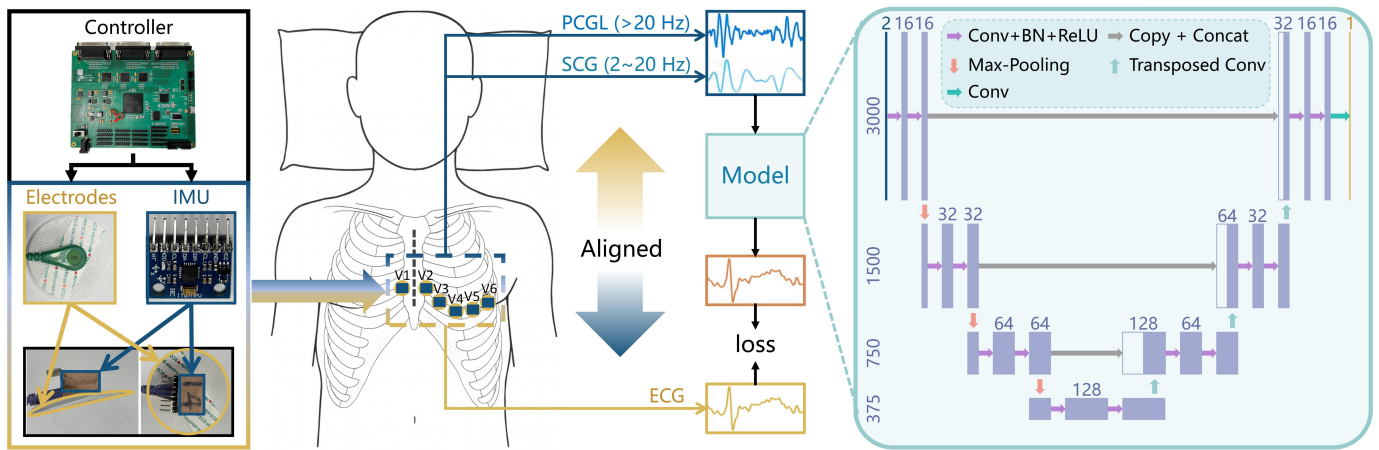


Fig. 2. The overview of the model and data collection approach. Left: In the hardware setup, an IMU is attached to an electrode buckle to form an electromechanical sensing pair that records colocated ECG and vibrational signals at six positions (V1–V6). All pairs are controlled by a single FPGA with a shared global clock, enabling timestamp-based interpolation for cross-modal alignment. Middle: The acquired vibration signals are decomposed into low-frequency signals (SCG, 2–20 Hz) and high-frequency phonocardiogram-like components (PCGL, >20 Hz), which are normalized separately and then together used as model inputs. Right: The baseline U-Net model takes SCG and PCGL as inputs to reconstruct the corresponding ECG signals, supervised by the aligned ground-truth ECG through a reconstruction loss.

RMSE of 0.081 mV, a median temporal error of 14 ms, and a median Pearson correlation of 90% with the ground truth waveform morphology.

Despite these advances, these studies have limitations. First, based on the manuals of their devices or dataset descriptions<sup>2</sup>, these studies are restricted to reconstructing ECG signals on limb leads from SCG collected at a fixed, single location. However, chest leads are essential for many cardiovascular diseases, such as myocardial infarction [41], ventricular fibrillation [42], congenital heart disease [43], ventricular tachycardia [44], and premature ventricular contraction [45]. Second, the SCG and ECG signals collected in these studies are unpaired, i.e., ECG is collected from the limbs while SCG is collected from the chest, wrist, or indirectly from a bed, which makes it incompatible with our goal that putting a single sensor or a mobile phone on the chest can lead to prediction of corresponding chest-lead ECG. Finally, none of these studies examined the temporal generalization of their models. Previous research [46] has indicated that it is unrealistic to expect a model trained on physiological data from a single day to perform well over an extended period, highlighting the need to investigate model performance over time, which requires multi-day data collection from the same subjects, a type of dataset that is currently lacking in this field.

Besides SCG, there are also studies using photoplethysmography (PPG) to reconstruct ECG [47]. However, the cost of PPG is not substantially lower than that of wearable ECG devices, limiting their advantage of cost-effectiveness for long-term ECG monitoring.

In summary, the main barrier to multi-lead-to-multi-lead conversion in SCG-to-ECG reconstruction is the lack of suitable paired datasets. To the best of our knowledge, this work

represents the first attempt to fill this gap. In contrast to prior studies that focus on single or limb-lead reconstruction using unpaired data, this work is the first to provide a paired, multi-location chest-lead SCG–ECG dataset with the potential to gain new insights into SCG-based applications and their relationship with ECG.

### III. METHODS

An overview of the model and data collection approach is illustrated in Fig. 2. This section first describes the hardware setup for data acquisition and the development of the dataset, followed by an introduction to data preprocessing, with a focus on the frequency-based decomposition method and its motivation from physiological and physical perspectives. Finally, the architecture of the benchmark model is presented.

#### A. Dataset and Hardware Setup for Data Acquisition

As a preliminary feasibility study, this work focuses primarily on healthy participants. Data were collected from 23 healthy male subjects aged between 21 and 70 years.<sup>3</sup> However, data from 6 participants were excluded due to severe electromagnetic interference near their acquisition sites, which caused excessive noise in their chest-lead ECG signals. Although the corresponding limb-lead ECG signals remained relatively clean, these data were not suitable for the objectives of this work and were therefore excluded from subsequent experiments. As a result, data from the remaining 17 participants with higher-quality precordial ECG and SCG signals were used for analysis.

Details of the signal acquisition system can be found in [48]. The system is capable of simultaneously recording SCG and ECG signals from 16 locations in the chest. In this study, 6 positions were used to cover the chest leads of the standard twelve-lead ECG system. At each position,

<sup>2</sup> [33] used the BioHarness 3.0 device to collect ECG data, which, according to its manual, records only one ECG channel. [34] used the CEBS dataset containing only lead I and lead II, both limb leads. [22] used the AD8232 ECG front end data sheet, which supports a single lead. [35] used the TI ADS1292 evaluation board manual, which has two channels. Measuring one chest lead requires at least four channels.

<sup>3</sup>All participants signed informed consent, permitting their data to be included in a shareable database.

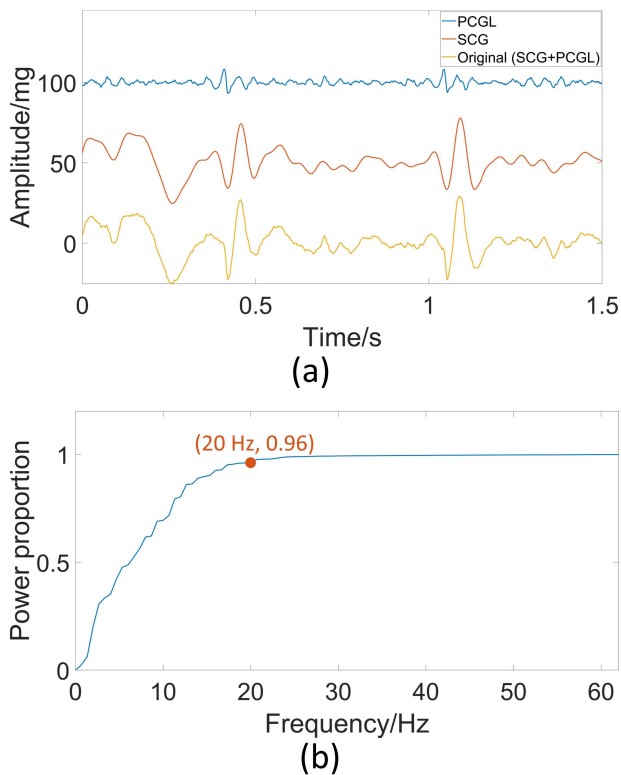


Fig. 3. SCG (0-20 Hz) contains over 96% of the total energy of the original signal. If the PCG-like (PCGL) component (above 20 Hz) is not separately extracted and normalized, it will be invisible within the original waveform, and the information carried in the PCGL band will be ignored.

an electrode was used to collect ECG signals, while an IMU for SCG acquisition was mounted directly above the electrode via the lead wire, ensuring that the collected SCG and ECG signals were paired. Both IMUs and analog-to-digital converters (ADCs) used for ECG acquisition were controlled by a field-programmable gate array (FPGA), with all device drivers sharing a global 50 MHz clock. This shared clock enabled precise cross-modal temporal alignment of ECG and SCG signals through timestamp-based interpolation, with an error below 20 ns.

During data collection, each participant was asked to lie supine on a bed. Each experimental session lasted 1.5 hours, with 1 hour dedicated to data recording. Participants were instructed to remain still and avoid speaking to minimize motion-induced interference in the SCG signals. Due to the duration of the experiment, most participants fell asleep during recording, and occasional snoring introduced additional noise into the SCG signals. In a few cases, brief speech occurred for unavoidable reasons, which may also have introduced transient motion artifacts.

### B. Data Preprocessing

In the data preprocessing pipeline, ECG signals were processed using a basic high-pass filter to remove baseline drift and a low-pass filter to eliminate power-line interference and its harmonics. Vibrational signals were similarly high-pass filtered to reduce motion artifacts.

Beyond noise removal, the vibrational signals were further decomposed into low-frequency SCG ( $< 20$  Hz) and high-

frequency Phonocardiography-like (PCGL,  $\geq 20$  Hz) components. The term “PCGL” is used because the waveform of the high-frequency component resembles that of phonocardiography (PCG) [49]. This separation is motivated by the complementary physiological information carried by the two components: SCG primarily reflects myocardial motion [13], while PCG is more sensitive to valve motion [50]. The cutoff frequency of 20 Hz was chosen because PCG is essentially an acoustic signal, and 20 Hz corresponds to the lower limit of human hearing, therefore, vibrational components above this frequency are treated as sound-related signals.

The necessity of separating SCG and PCGL is illustrated in Fig. 3. As shown in Fig. 3(a), the amplitude of PCGL is smaller than that of SCG, and the original signal, which contains both SCG and PCGL, closely resembles the SCG waveform. This indicates that if PCGL is not separately extracted and normalized, feeding the original signal directly into a model is nearly equivalent to using SCG alone, and the information carried by PCGL will be ignored. Fig. 3(b) further quantifies this observation: after removing the direct current (DC) component, the energy of the vibrational signal above 20 Hz accounts for less than 4% of the total energy, further highlighting the necessity of extracting and normalizing the high-frequency component.

After the noise removal and vibrational signal decomposition, we align the vibrational signals with the ECG signals through interpolation. Considering hardware constraints, communication rate, and signal-to-noise ratio, the ECG ADC sampling rate is set to a higher value of 1000 Hz, while the IMU sampling rate is set to 500 Hz, resulting in misaligned sampling instances between the two modalities. However, as described in the previous subsection, the ADC and IMU drivers share the same clock on the FPGA, and both modalities transmit their data together with the corresponding timestamps to the upper computer. This allows interpolation-based alignment of the two modalities using the timestamps. In this study, taking the ECG timestamps as the reference, the SCG and PCGL signals are interpolated to 1000 Hz for alignment.

### C. Model

Our baseline model is constructed based on Wave U-Net [51], which was originally developed for audio source separation. The architecture and its variants have subsequently been shown to be effective for physiological signal reconstruction [47], [52]–[54], making it suitable as a baseline model for validating the feasibility of the ECG reconstruction task in this study. In addition, compared with other architectures directly used for SCG-to-ECG conversion, such as GANs and Transformers [22], [34], [35], Wave U-Net is more lightweight. Compared with LSTM-based models [33], Wave U-Net, as a fully convolutional network, enables efficient parallel computation and results in lower computational latency [55]. These characteristics make Wave U-Net more suitable for the target application scenario of this study, namely, ECG reconstruction on low-cost mobile devices.

The model architecture is shown in Fig. 2. The network adopts an encoder–decoder structure with symmetric skip connections. The input consists of two channels, corresponding to

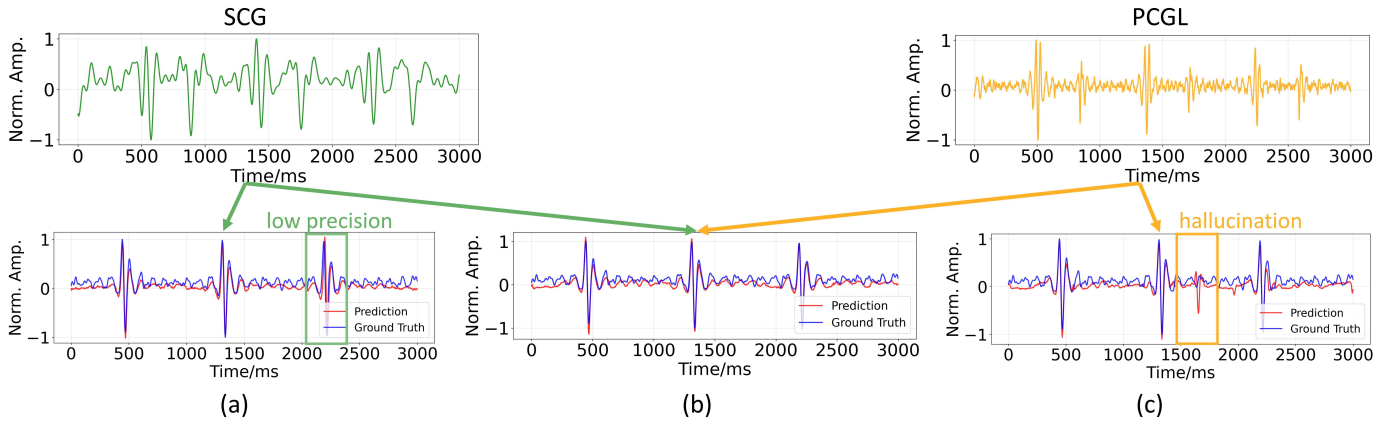


Fig. 4. A typical comparative example with different inputs. (a) Reconstruction with only SCG as input. The outputs are less precise in amplitude and timing but exhibit fewer hallucinations, i.e., generated ECG waveforms that do not actually exist. (b) Reconstruction with SCG and PCGL as inputs. The outputs are precise and exhibit fewer hallucinations. (c) Reconstruction with only PCGL as input. The outputs are more precise but exhibit more hallucinations.

the low-frequency SCG (2–20 Hz) and high-frequency PCGL (>20 Hz) signals, each with a length of 3000 samples (3 s).

In the encoder, each layer contains two convolutional blocks, each composed of a 1D convolution with a kernel size of 7, batch normalization, and ReLU activation, followed by down-sampling using max-pooling with a factor of 2. The number of feature channels progressively increases as the network goes deeper, eventually reaching 128.

In the decoder, the temporal resolution is restored using transposed convolutions, and the corresponding encoder features are concatenated via skip connections (copy-and-concatenate) to preserve fine-grained temporal information. Each layer of the decoder has the same convolutional blocks as the encoder. In the last layer, a convolution with a kernel size of 1 is used for feature fusion to generate the final prediction of ECG signals.

#### IV. EXPERIMENTAL EVALUATION AND RESULTS

In this section, we first describe the experimental setup and evaluation metrics, then present an ablation study on input decomposition and experiment results on temporal generalization, and finally analyze the causes of hallucination based on these results.

##### A. Experimental Setup for Model Training and Testing

In this study, training and testing were conducted in a subject-specific approach. For each subject’s (participant’s) data, the dataset was divided based on time, with the earliest 70% of the data used for training, the middle 10% for validation, and the last 20% for testing. The model that achieved the best performance on the validation set was selected for testing to prevent data leakage.

The utilized model accuracy metric is the L1 distance, because compared with other metrics such as correlation-based loss or dynamic time warping, it imposes stricter requirements on both amplitude and temporal precision, while also being more intuitive and easier to interpret. In addition, to quantify the severity of model hallucination, we randomly selected 310 reconstructed ECG signals from the test results and manually

counted the occurrences of hallucinations. The total number of reconstructed ECG signals in each test result ranged from 1200 to 1450. Therefore, the manually inspected 310 reconstructed ECG signals ensured statistical significance ( $p < 0.05$ ).

##### B. Ablation Study on Input Decomposition

In this section, we present the model accuracy with different inputs. As shown in Fig. 4, comparing (a), (b), and (c) reveals that when the input contains only an SCG signal, the output exhibits lower precision in amplitude and timing but shows a lower likelihood of hallucination, i.e., generate a fake ECG waveform that does not exist. When the input contains only a PCGL signal, the output becomes more precise but hallucination occurs more frequently. When the input contains both SCG and PCGL signals, the accuracy is improved and the hallucination is diminished.

The quantitative results are shown in Fig. 5(a) and (b). In Fig. 5(a), for most subjects, the hallucination frequency is the highest when only PCGL is used as input, followed by the case where only SCG is used. In Fig. 5(b), for most subjects, the average L1 distance for a subject is the largest when only SCG is used as input, indicating lower precision. In contrast, when normalized PCGL and SCG are jointly used as two input channels (denoted as “Both”), both the hallucination frequency and the prediction precision are minimized, indicating that both high-frequency and low-frequency components are informative to this task.

In Fig. 5(a) and (b), we also include a comparison using the raw signal as input (denoted as “Raw”), i.e., the original acceleration signal without decomposition. For most subjects, in terms of hallucination frequency, the performance of the raw signal is close to that of SCG and substantially worse than that of “Both”. In terms of precision, the raw signal performs slightly worse than “Both”. This further demonstrates that frequency-based decomposition and normalization of the input signals improve the model performance.

It is worth mentioning that in this experiment, switching the input from a single channel to two channels only changes the number of parameters in the first convolutional layer. Specifically, the model with two input channels adds only

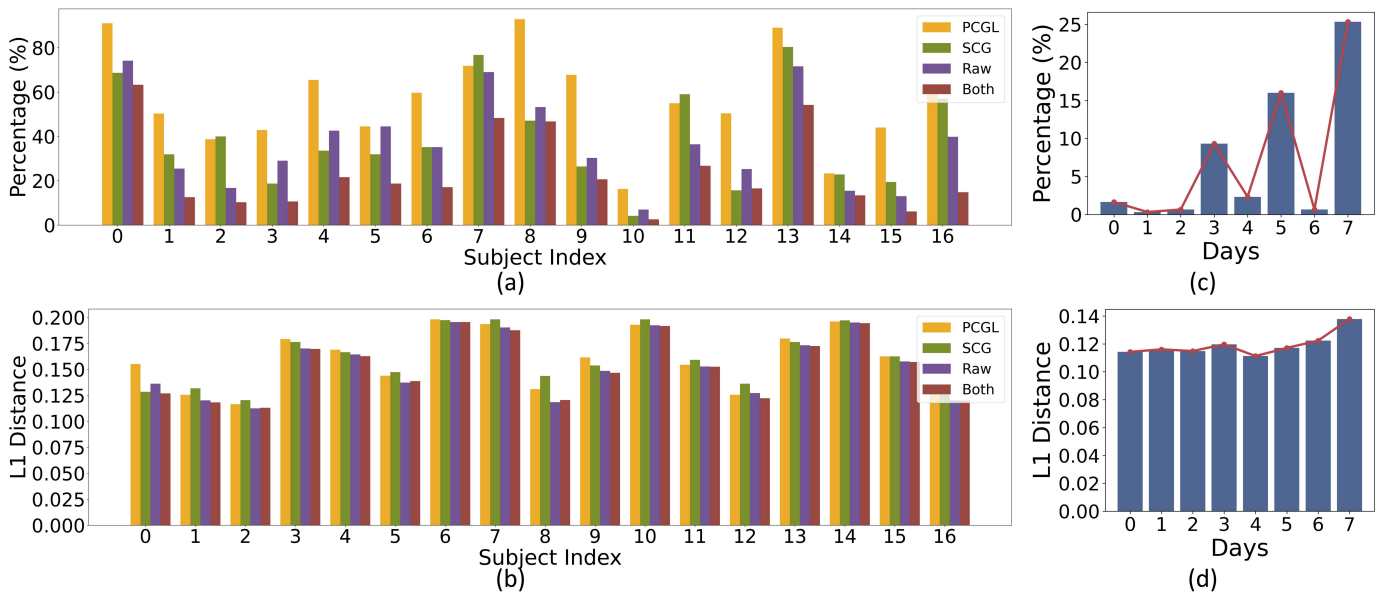


Fig. 5. (a) Hallucination percentage with different inputs. “PCGL” and “SCG” denote models using a single normalized PCGL or SCG channel as input, respectively. “Raw” indicates the use of a single channel of the original acceleration signal without decomposition. “Both” represents a two-channel input consisting of normalized PCGL and SCG signals. (b) L1 distance with different inputs. (c) Hallucination percentage with different time interval between training and testing data. (d) L1 distance with different time interval between training and testing data.

$(2 - 1) \times 16 \times 7 = 112$  parameters compared to the single-channel model. This increase is negligible relative to the total model size of 364 K parameters. Therefore, the performance improvement can be attributed entirely to the change in input.

### C. Temporal Generalization Experiment

Intuitively, it is impractical to expect a model trained on data collected on a single day to remain effective over a long period. Therefore, unlike previous studies, in this work, the temporal generalization of the trained model is investigated. A subject was selected and data were collected continuously over 8 days. Each recording session was conducted at approximately the same time of day, resulting in an interval of about 24 hours between data from consecutive days. In this experiment, the data from the first day were used for training and testing following the procedure described in Section IV-A, while the data from each subsequent day were used only for testing.

The experimental results are shown in Fig. 5(c) and (d). It can be observed that both the hallucination frequency and the L1 distance exhibit oscillatory trends over time rather than monotonic increases or decreases. This suggests that, over a short-term period (one week), the occurrence of hallucinations is not dominated by the temporal gap between the training and testing data. In particular, the test results on the third, fifth, and seventh days show a noticeably higher number of hallucinations. Based on an inspection of the data from these days, we attribute the increased hallucination frequency mainly to noise, such as involuntary body movements, coughing or vocalization by the subject.

### D. Causes of Hallucination

By analyzing the results of the experiments in the previous two sections, three main categories of causes can be identified: noise interference, misclassification of the second heart sound

(S2) as the first heart sound (S1), and semantic loss at segment boundaries. Typical examples are illustrated in Fig. 6.

Noise interference is the primary cause of hallucinations. Noise obscures the waveforms corresponding to cardiac systole and diastole in SCG and PCGL signals, making it difficult to determine when, or even whether, a heartbeat has occurred, thereby inducing hallucinations. In addition to the factors mentioned in the previous subsection, such as body movement, coughing, and vocalization, the primary source of noise is snoring. For subjects with relatively severe snoring, namely Subjects 7, 8, and 13, Fig. 5(a) shows that their hallucination frequencies are at least 20% higher than those of other subjects. It is worth noting Subject 0, whose data are not affected by snoring but still exhibit a higher hallucination frequency. A possible explanation is that this subject has relatively weak cardiac contractions combined with thicker subcutaneous fat, resulting in vibration signals with smaller amplitudes that are difficult for the model to capture, thereby leading to a high hallucination frequency.

Misclassification of the second heart (S2) sound as the first heart (S1) sound can explain why using only PCGL as input produces more hallucinations than using only SCG. S1 mainly originates from vibrations caused by the closure of the mitral and tricuspid valves and marks the onset of ventricular systole, whereas S2 mainly originates from vibrations caused by the closure of the aortic and pulmonary valves and marks the onset of ventricular diastole. In PCGL signals, the waveforms of S1 and S2 are similar in shape, with the primary difference being that the amplitude of S1 is generally larger than that of S2. However, this distinction is not reliable. For nearly every subject, there exist cardiac cycles in which the amplitude of S2 approaches that of S1, or cases where, although the S2 amplitude is smaller than S1 within the same cycle, it is comparable to or even exceeds the S1 amplitude in other

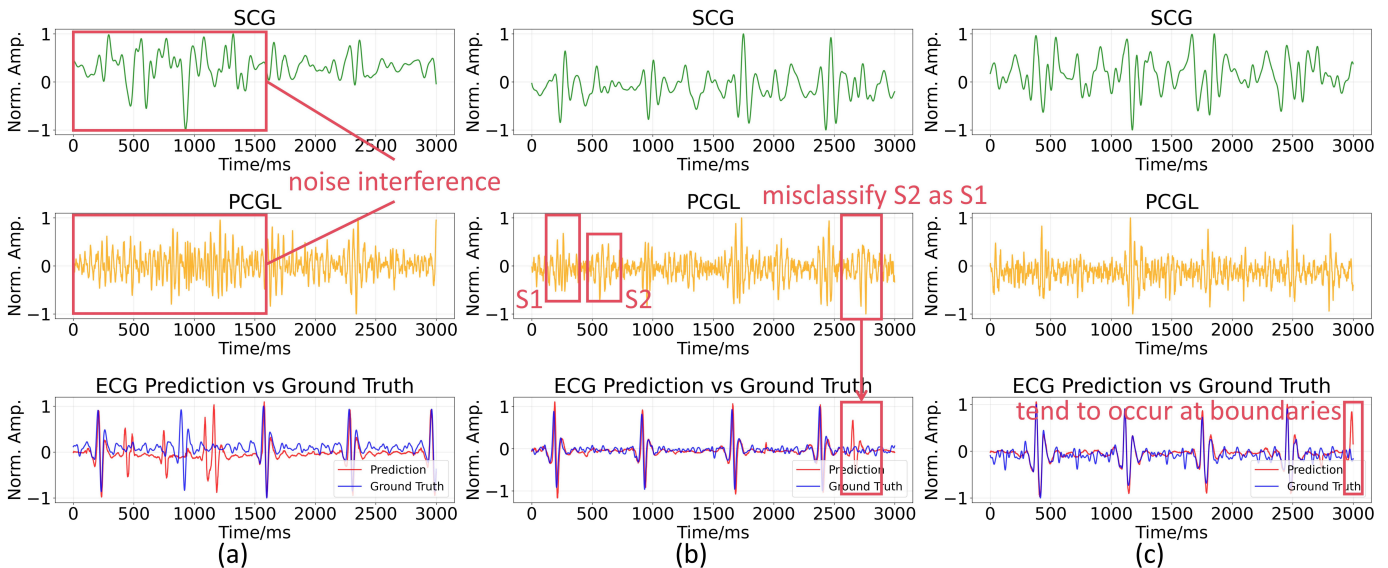


Fig. 6. Factors contributing to the occurrence of hallucinations: (a) noise interference, (b) misclassification of the second heart sound (S2) as the first heart sound (S1), and (c) semantic loss at segment boundaries.

cardiac cycles. In contrast, SCG waveforms during systole and diastole differ in both shape and amplitude and are less prone to confusion. Therefore, in the absence of SCG as a reference input, the similarity between S1 and S2 in PCGL can confuse the model, causing it to generate an ECG waveform during diastole that should have appeared during systole. Moreover, hallucinations induced by this mechanism tend to have more complete waveforms and larger amplitudes compared with those caused by noise.

In addition to the two causes discussed above, hallucinations also tend to occur at segment boundaries. We assume that this is because the model cannot observe complete waveforms and sufficient contextual information at the boundaries, leading to errors in determining whether a heartbeat is present.

## V. DISCUSSION

This section first discusses possible directions for mitigating model hallucination, then presents insights gained from this study, including the significance of high-frequency components in vibration signals and the potential for deployment on mobile devices, and finally explores other possible applications of the dataset.

### A. Potential Directions for Mitigating Model Hallucination

1) *Improving Input Signal Quality*: Improving the input signal quality is the most direct way to mitigate hallucinations. As explained in Section IV-D, when the input signal quality is sufficient to provide reliable information indicating cardiac systole and diastole, the hallucination frequency decreases significantly. In addition, our observations indicate that the occurrence of hallucinations is not strongly correlated with the training data label quality, i.e., the noise level of the ECG reference signal. Fig. 7 shows a representative data segment from Subject 10. In this subject’s data, the ECG signal (the blue curve in the figure) contains relatively substantial noise, which results in a relatively large L1 distance compared

with most other subjects, as shown in Fig. 5(b). However, the input SCG and PCGL signal quality for this subject is relatively high—specifically, at least one input channel exhibits clearly discernible periodic waveforms—leading to the lowest hallucination frequency among all subjects, as shown in Fig. 5(a). The testing results from Subject 10 further emphasize that improving the input data quality can effectively reduce the hallucination frequency, even when the label quality is relatively poor.

2) *Correlate R-peak and Heart Sounds*: A second major contributor to hallucinations is confusion between S2 and S1, which is particularly pronounced when using only PCGL as input. Compared with noise-induced hallucinations, these cases are often easier to identify because they tend to occur temporally close to S2 and far from the expected timing of S1, and they frequently resemble true QRS complexes with larger and more complete waveforms. A practical mitigation strategy is to enforce a physiological consistency check between heart sounds and predicted R-peaks. Specifically, S2 can be detected from the input PCGL signal, while QRS complex or R-peak detection is applied to the reconstructed ECG. Hallucinations can then be flagged when an R-peak occurs in an implausible temporal relationship with detected heart sounds (e.g., abnormally close to S2 or outside an expected timing window). The key components of this strategy, namely QRS detection and heart sound detection, have been extensively studied and are supported by mature algorithms, such as those in [56] and [57]. Therefore, this issue is theoretically solvable.

### B. Significance of High-Frequency Components

In signal processing, smoother signals are often intuitively preferred, and waveform “spikes” are typically regarded as undesirable, which often leads to the removal of high-frequency components. SCG signals are no exception, and previous studies, such as [22], [33], explicitly retained only the frequency range between 5 and 30 Hz. Only a limited number of works

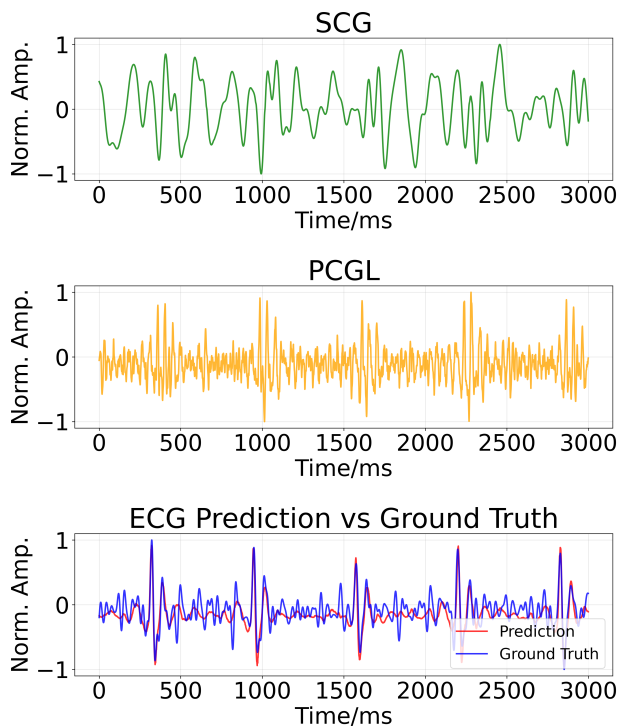


Fig. 7. Results from Subject 10 demonstrate that as long as the input signal quality is sufficient for the model to obtain enough information to determine whether and when a heartbeat occurs, no hallucinations are produced in the output, even when the ECG signal used as ground truth contains substantial noise.

have explicitly noted that high-frequency components may serve as a useful complement to SCG signals [49]. In our study, the ablation analysis provides further evidence of the potential value of high-frequency components, namely PCGL, highlighting that components often regarded as noise may provide informative clues for SCG-related tasks.

### C. Potential of Applications on Mobile Devices

Our results suggest that simultaneously and synchronously acquired ECG and vibrational signals (including SCG and PCGL) at the same chest location provide strong temporal and physiological alignment, which helps the model learn more cross-modal correlated features, without relying on structurally complex or computationally intensive model architectures. Compared with previous SCG-to-ECG studies using models such as GAN, Transformer, or Bi-LSTM [22], [33]–[35], this work employs a lightweight Wave U-Net with only 364 K parameters, making it more suitable for resource-constrained and mobile-device scenarios. This design also aligns with the intended use case: placing a mobile device with an IMU (e.g. a smartphone) on the chest to directly reconstruct the corresponding chest-lead ECG signal. Compared with configurations limited to one or two fixed limb leads in prior studies, the proposed lead configuration has the potential to offer improved clinical relevance, enhanced flexibility, and value, while enabling low-cost, convenient, on-device ECG monitoring in practical settings.

### D. Other Potential Uses of the Dataset

In addition to build a model for reconstruction of ECG from SCG signals, our dataset can also be used for other purposes. Potential applications are described as follows:

1) *Electromechanical Coupling Analysis*: As ECG and SCG signals in our dataset are collected synchronously at the chest-lead positions of the standard twelve-lead ECG system, the dataset provides an opportunity to investigate the electromechanical coupling relation between SCG and ECG and the corresponding physiological activities from a medical perspective, thus provides support for SCG interpretation.

2) *Optimal Position for Single-Channel Wearable SCG*: For wearable SCG applications that rely on a single sensor, choosing an optimal placement location is critical, as signal quality and waveform morphology can vary substantially across chest positions. Previous studies typically repeated experiments by placing a single sensor at different positions sequentially, which may introduce confounding effects due to subject fatigue, posture changes, or adaptation across repeated trials and thus affect experimental results. In contrast, our dataset provides SCG signals recorded synchronously at multiple chest locations, enabling fair comparisons of candidate placements under matched physiological and behavioral conditions.

3) *Denosing*: Long-term cardiac monitoring studies, particularly during sleep, inevitably involve sleep-related artifacts such as snoring and involuntary body movements. During the data collection process of this dataset, most subjects fell asleep, resulting in recordings that naturally contain sleep-related noises. Therefore, this dataset can support research on SCG signal denoising, thereby facilitating long-term cardiac monitoring, particularly for sleep-related cardiac monitoring applications scenarios.

## VI. LIMITATIONS AND FUTURE WORK

### A. Limitations

As an exploratory study, this work has several limitations. First, being constrained by the equipment and experimental environment, the overall quality of the ECG signals used as ground truth is not ideal. This primarily affects the precision of the quantitative performance evaluation, but does not undermine the feasibility of the proposed cross-modal reconstruction framework. Second, commonly used metrics in prior studies, such as correlation-based loss or dynamic time warping loss, are not sensitive to the hallucination phenomenon identified in this work. As a result, manual inspection and counting were adopted to estimate the hallucination frequency. Although effective, this approach is time-consuming and may introduce subjective bias. Third, the temporal generalization experiment was conducted on data from a single subject due to the high cost and complexity of long-term data collection. While the results provide preliminary insights, the limited sample size prevents more general conclusions regarding long-term robustness.

### B. Future Work

This study demonstrates the feasibility of converting cardiac vibrational signals into ECG signals using lightweight models. Based on this work, several directions can be further explored:

1) *Adapting Spiking Neural Networks*: As analyzed in Sections IV-D and V-A, reconstructing ECG signals may primarily rely on information such as the timing of cardiac beats. This suggests that the informative content in SCG and PCGL signals is sparse, which is well suited for spiking neural networks (SNNs). Therefore, a potential direction is to identify critical features and encode the inputs into spikes accordingly for processing, thereby further improving computing efficiency.

2) *Vibrational Signal Denoising*: The analyses in Sections IV-D and V-A indicate that the input signal quality is the dominant factor affecting the model performance. Accordingly, a promising direction is to develop denoising algorithms for the input signals, such as methods to suppress interference caused by snoring.

3) *Enhancing the Dataset and Evaluation Metrics*: Future work will also focus on expanding the dataset, particularly by collecting long-term recordings from multiple subjects to enable more comprehensive temporal generalization analysis. In addition, developing objective and automatically computable metrics for hallucination evaluation is an important direction.

## VII. CONCLUSION

This work presents the first dataset comprising paired vibrational signals and ECG signals collected at chest-lead positions of the standard twelve-lead system. Using this dataset, we demonstrate the feasibility of training and using a lightweight neural network model to reconstruct corresponding ECG signals from cardiac vibrational signals at variable locations through experiments. We further analyze the hallucination phenomenon of the model, identify its primary causes, and provide potential mitigation strategies.

The low acquisition cost of acceleration-based signals and the widespread clinical use of the twelve-lead ECG system support the application potential of this study and the released dataset. Moreover, the lightweight U-Net model employed in this work, containing only 364 K parameters, further suggests the feasibility of deploying such models on mobile devices without requiring additional hardware. This reveals a potential vision in which a mobile device equipped with an IMU, such as a smartphone, can be placed on the chest to automatically reconstruct the corresponding chest-lead ECG signal, significantly reducing the hardware cost while preserving the clinical relevance of the reconstructed ECG signal. This approach opens new possibilities for large-scale, long-term, and more interpretable cardiac monitoring.

## REFERENCES

- [1] D. P. Zipes, *Braunwald's heart disease e-book: A textbook of cardiovascular medicine*. Elsevier Health Sciences, 2018.
- [2] R. Wang, S. C. M. Veera, O. Asan, and T. Liao, "A systematic review on the use of consumer-based ecg wearables on cardiac health monitoring," *IEEE Journal of Biomedical and Health Informatics*, 2024.
- [3] O. Jaradat, P. Drury, J. Rihari-Thomas, and S. Frost, "Non-invasive monitoring strategies for atrial fibrillation detection in adult cardiac surgery patients after hospital discharge: A scoping review," *Heart & Lung*, vol. 73, pp. 9–18, 2025.
- [4] J. Lázaro, N. Reljin, R. Bailón, E. Gil, Y. Noh, P. Laguna, and K. H. Chon, "Tracking tidal volume from holter and wearable armband electrocardiogram monitoring," *IEEE journal of biomedical and health informatics*, vol. 28, no. 6, pp. 3457–3465, 2024.
- [5] W. Zhu, X. Bian, and J. Lv, "From genes to clinical management: A comprehensive review of long qt syndrome pathogenesis and treatment," *Heart Rhythm O2*, vol. 5, no. 8, pp. 573–586, 2024.
- [6] C. Jons, P. Sogaard, S. Behrens, J. Schrader, S. Mrosk, and P. E. Bloch Thomsen, "The clinical effect of arrhythmia monitoring after myocardial infarction (bio-guard—mi): study protocol for a randomized controlled trial," *Trials*, vol. 20, no. 1, p. 563, 2019.
- [7] C. L. Chow, H.-C. Han, A. W. Teh, R. P. Lim, H. Salehi, A. N. Koshy, D. L. Hare, P. Sanders, O. Farouque, and H. S. Lim, "Continuous rhythm monitoring and signal-averaged electrocardiogram to risk stratify ventricular arrhythmia in mitral valve prolapse," *JACC: Advances*, vol. 4, no. 4, p. 101643, 2025.
- [8] J. Zhang, Y. Guo, X. Dong, T. Wang, J. Wang, X. Ma, and H. Wang, "Opportunities and challenges of noise interference suppression algorithms for dynamic ecg signals in wearable devices: A review," *Measurement*, p. 117067, 2025.
- [9] O. Freund, I. Caspi, I. Alcalay, M. R. Brezis, S. Frydman, and G. Bornstein, "An old diagnostic tool for new indications: inpatient holter ecg for conditions other than syncope or stroke," *Scientific Reports*, vol. 13, no. 1, p. 12510, 2023.
- [10] S. Hyun, S. Lee, Y. S. Hong, S.-h. Lim, and D. J. Kim, "Evaluation of the diagnostic performance and efficacy of wearable electrocardiogram monitoring for arrhythmia detection after cardiac surgery," *Journal of Chest Surgery*, vol. 57, no. 2, p. 205, 2024.
- [11] K. Sørensen, S. E. Schmidt, A. S. Jensen, P. Sogaard, and J. J. Struijk, "Definition of fiducial points in the normal seismocardiogram," *Scientific reports*, vol. 8, no. 1, p. 15455, 2018.
- [12] C. Yang and N. Tavassolian, "Combined seismo-and gyro-cardiography: A more comprehensive evaluation of heart-induced chest vibrations," *IEEE journal of biomedical and health informatics*, vol. 22, no. 5, pp. 1466–1475, 2017.
- [13] D. Rai, H. K. Thakkar, S. S. Rajput, J. Santamaria, C. Bhatt, and F. Roca, "A comprehensive review on seismocardiogram: current advancements on acquisition, annotation, and applications," *Mathematics*, vol. 9, no. 18, p. 2243, 2021.
- [14] A. Agam, A. Agam, E. Korsgaard, T. Yding, C. B. Kristensen, R. Mogelvang, K. Kragholm, K. J. G. Emerk, P. Sogaard, and S. E. Schmidt, "Evaluation of seismocardiography in detecting pre-load changes and cardiovascular disease: a comparative study with transthoracic echocardiography," *European Heart Journal-Digital Health*, p. ztaf037, 2025.
- [15] A. Taebi, B. E. Solar, A. J. Bomar, R. H. Sandler, and H. A. Mansy, "Recent advances in seismocardiography," *Vibration*, vol. 2, no. 1, pp. 64–86, 2019.
- [16] Y. Liu, Z. Li, S. Zheng, P. Cai, and X. Zou, "An evaluation of mems-imu performance on the absolute trajectory error of visual-inertial navigation system," *Micromachines*, vol. 13, no. 4, p. 602, 2022.
- [17] K. Kulkarni, R. K. Sevakula, M. B. Kassab, J. Nichols, J. D. Roberts Jr, E. M. Isselbacher, and A. A. Aroundas, "Ambulatory monitoring promises equitable personalized healthcare delivery in underrepresented patients," *European Heart Journal-Digital Health*, vol. 2, no. 3, pp. 494–510, 2021.
- [18] A. Hossein, E. Abdessater, P. Balali, E. Cosneau, D. Gorlier, J. Rabineau, A. Almorad, V. Faoro, and P. Van De Borne, "Smartphone-derived seismocardiography: Robust approach for accurate cardiac energy assessment in patients with various cardiovascular conditions," *Sensors*, vol. 24, no. 7, p. 2139, 2024.
- [19] U.-V. Albrecht, D. Lawin, S. Kuhn, and U. Kulau, "Seismocardiography with smartphones: no leap from bench to bedside (yet)," *Advances in Informatics, Management and Technology in Healthcare*, pp. 271–275, 2022.
- [20] O. Lahdenoja, T. Hurnanen, Z. Iftikhar, S. Nieminen, T. Knuutila, A. Saraste, T. Kiviniemi, T. Vasankari, J. Airaksinen, M. Pänkäälä et al., "Atrial fibrillation detection via accelerometer and gyroscope of a smartphone," *IEEE journal of biomedical and health informatics*, vol. 22, no. 1, pp. 108–118, 2017.
- [21] A. M. Carek, J. Conant, A. Joshi, H. Kang, and O. T. Inan, "Seismowatch: wearable cuffless blood pressure monitoring using pulse transit time," *Proceedings of the ACM on interactive, mobile, wearable and ubiquitous technologies*, vol. 1, no. 3, pp. 1–16, 2017.
- [22] Y. Cao, F. Li, H. Chen, X. Liu, L. Zhang, and Y. Wang, "Guard your heart silently: Continuous electrocardiogram waveform monitoring with wrist-worn motion sensor," *Proceedings of the ACM on Interactive, Mobile, Wearable and Ubiquitous Technologies*, vol. 6, no. 3, pp. 1–29, 2022.
- [23] J. M. Zanetti and K. Tavakolian, "Seismocardiography: Past, present and future," in *2013 35th annual international conference of the IEEE*

- engineering in medicine and biology society (EMBC)*. IEEE, 2013, pp. 7004–7007.
- [24] M. M. H. Shandhi, B. Semiz, S. Hersek, N. Goller, F. Ayazi, and O. T. Inan, “Performance analysis of gyroscope and accelerometer sensors for seismocardiography-based wearable pre-ejection period estimation,” *IEEE journal of biomedical and health informatics*, vol. 23, no. 6, pp. 2365–2374, 2019.
- [25] J. Skoric, Y. D’Mello, and D. V. Plant, “A wavelet-based approach for motion artifact reduction in ambulatory seismocardiography,” *IEEE Journal of Translational Engineering in Health and Medicine*, vol. 12, pp. 348–358, 2024.
- [26] B. Semiz, A. M. Carek, J. C. Johnson, S. Ahmad, J. A. Heller, F. G. Vicente, S. Caron, C. W. Hogue, M. Etemadi, and O. T. Inan, “Non-invasive wearable patch utilizing seismocardiography for peri-operative use in surgical patients,” *IEEE journal of biomedical and health informatics*, vol. 25, no. 5, pp. 1572–1582, 2020.
- [27] L. Liu, D. Yu, H. Lu, C. Shan, and W. Wang, “Camera-based seismocardiogram for heart rate variability monitoring,” *IEEE Journal of Biomedical and Health Informatics*, vol. 28, no. 5, pp. 2794–2805, 2024.
- [28] V. G. Ganti, A. H. Gazi, S. An, A. V. Srivatsa, B. N. Nevius, C. J. Nichols, A. M. Carek, M. Fares, M. Abdulkarim, T. Hussain *et al.*, “Wearable seismocardiography-based assessment of stroke volume in congenital heart disease,” *Journal of the American Heart Association*, vol. 11, no. 18, p. e026067, 2022.
- [29] J. P. Kimball, J. S. Zia, S. An, C. Rolfes, J.-O. Hahn, M. N. Sawka, and O. T. Inan, “Unifying the estimation of blood volume decompensation status in a porcine model of relative and absolute hypovolemia via wearable sensing,” *IEEE Journal of Biomedical and Health Informatics*, vol. 25, no. 9, pp. 3351–3360, 2021.
- [30] M. Chan, V. G. Ganti, and O. T. Inan, “Respiratory rate estimation using u-net-based cascaded framework from electrocardiogram and seismocardiogram signals,” *IEEE journal of biomedical and health informatics*, vol. 26, no. 6, pp. 2481–2492, 2022.
- [31] I. Elnaggar, T. Hurnanen, O. Lahdenoja, A. Airola, M. Kaisti, T. Vasankari, J. Pykärä, M. Savontaus, and T. Koivisto, “Detecting aortic stenosis using seismocardiography and gryocardiography combined with convolutional neural networks,” in *2021 Computing in Cardiology (CinC)*, vol. 48. IEEE, 2021, pp. 1–4.
- [32] M. M. H. Shandhi, W. H. Bartlett, J. A. Heller, M. Etemadi, A. Young, T. Plötz, and O. T. Inan, “Estimation of instantaneous oxygen uptake during exercise and daily activities using a wearable cardio-electromechanical and environmental sensor,” *IEEE journal of biomedical and health informatics*, vol. 25, no. 3, pp. 634–646, 2020.
- [33] J. Park, H. Cho, R. K. Balan, and J. Ko, “Heartquake: Accurate low-cost non-invasive ecg monitoring using bed-mounted geophones,” *Proceedings of the ACM on Interactive, Mobile, Wearable and Ubiquitous Technologies*, vol. 4, no. 3, pp. 1–28, 2020.
- [34] Neeraj, U. Satija, J. Mathew, R. Behera *et al.*, “A unified attentive cycle-generative adversarial framework for deriving electrocardiogram from seismocardiogram signal,” *IEEE signal processing letters*, vol. 29, pp. 802–806, 2022.
- [35] J. Chen, D. Zhang, Z. Wu, F. Zhou, Q. Sun, and Y. Chen, “Contactless electrocardiogram monitoring with millimeter wave radar,” *IEEE Transactions on Mobile Computing*, vol. 23, no. 1, pp. 270–285, 2022.
- [36] E. R. Pfeiffer, J. R. Tangney, J. H. Omens, and A. D. McCulloch, “Biomechanics of cardiac electromechanical coupling and mechano-electric feedback,” *Journal of biomechanical engineering*, vol. 136, no. 2, 2014.
- [37] F. W. Prinzen, K. Vernooy, B. W. DeBoeck, and T. Delhaas, “Mechano-energetics of the asynchronous and resynchronized heart,” *Heart failure reviews*, vol. 16, no. 3, pp. 215–224, 2011.
- [38] J. Bacevicius, N. Taparauskaite, R. Kundelis, D. Sokas, M. Butkuviene, G. Stankeviciute, Z. Abramikas, A. Pilkiene, E. Dvinelis, J. Staigyte *et al.*, “Six-lead electrocardiography compared to single-lead electrocardiography and photoplethysmography of a wrist-worn device for atrial fibrillation detection controlled by premature atrial or ventricular contractions: six is smarter than one,” *Frontiers in Cardiovascular Medicine*, vol. 10, p. 1160242, 2023.
- [39] G.-W. Yoon and S. Joo, “Classification feasibility test on multi-lead electrocardiography signals generated from single-lead electrocardiography signals,” *Scientific Reports*, vol. 14, no. 1, p. 1888, 2024.
- [40] A. Zepeda-Echavarría, R. R. van de Leur, M. Vessies, N. M. de Vries, M. van Sleuwen, R. J. Hassink, T. X. Wildbergh, J. van Doorn, R. van Zee, P. A. Doevendans *et al.*, “Detection of acute coronary occlusion with a novel mobile electrocardiogram device: a pilot study,” *European Heart Journal-Digital Health*, vol. 5, no. 2, pp. 183–191, 2024.
- [41] H. Namdar, L. Imani, S. Ghaffari, N. Aslanabadi, N. Reshadati, Z. Samani, G. Davarmoin, N. Moayyednia, Y. Nazer, S. Sarhangzadeh *et al.*, “St-segment depression in left precordial leads in electrocardiogram of patients with acute inferior myocardial infarction undergoing primary percutaneous coronary intervention,” *Interventional Medicine and Applied Science*, vol. 10, no. 4, pp. 191–197, 2018.
- [42] Y. Nakano, W. Shimizu, H. Ogi, K. Suenari, N. Oda, Y. Makita, K. Kajihara, Y. Hirai, A. Sairaku, T. Tokuyama *et al.*, “A spontaneous type 1 electrocardiogram pattern in lead v2 is an independent predictor of ventricular fibrillation in brugada syndrome,” *Europace*, vol. 12, no. 3, pp. 410–416, 2010.
- [43] M. White, M. Gormley, E. Jimenez, M. Evans, and B. Clark, “Diagnostic utility of prominent mid-precordial lead voltage in a pediatric population,” *Pediatric Cardiology*, pp. 1–5, 2025.
- [44] C. Reithmann, M. Fiek, Z. Aynur, and M. Ulbrich, “Electrocardiographic criteria of epicardial ventricular tachycardia with anterior origin,” *Clinical Research in Cardiology*, vol. 108, no. 3, pp. 254–263, 2019.
- [45] T. Yamada, “Twelve-lead electrocardiographic localization of idiopathic premature ventricular contraction origins,” *Journal of cardiovascular electrophysiology*, vol. 30, no. 11, pp. 2603–2617, 2019.
- [46] J. Cano, V. Bertomeu-González, L. Fácila, F. Hornero, R. Alcaraz, and J. J. Rieta, “Improved hypertension risk assessment with photoplethysmographic recordings combining deep learning and calibration,” *Bioengineering*, vol. 10, no. 12, p. 1439, 2023.
- [47] Q. Tang, Z. Chen, R. Ward, C. Menon, and M. Elgendi, “Ppg2ecggs: An end-to-end subject-specific deep neural network model for electrocardiogram reconstruction from photoplethysmography signals without pulse arrival time adjustments,” *Bioengineering*, vol. 10, no. 6, p. 630, 2023.
- [48] G. Lu, K. Chen, Q. Wang, and X. Cai, “Dual-modality electromechanical physiology source mapping,” *IEEE Sensors Journal*, vol. 24, no. 10, pp. 16 387–16 396, 2024.
- [49] F. Khosrow-Khavar, K. Tavakolian, A. P. Blaber, J. M. Zanetti, R. Fazel-Rezai, and C. Menon, “Automatic annotation of seismocardiogram with high-frequency precordial accelerations,” *IEEE journal of biomedical and health informatics*, vol. 19, no. 4, pp. 1428–1434, 2014.
- [50] A. K. Bhoi, K. S. Sherpa, and B. Khandelwal, “Multidimensional analytical study of heart sounds: A review,” *International Journal Bioautomation*, vol. 19, no. 3, p. 351, 2015.
- [51] D. Stoller, S. Ewert, and S. Dixon, “Wave-u-net: A multi-scale neural network for end-to-end audio source separation,” *arXiv preprint arXiv:1806.03185*, 2018.
- [52] X. Xiang, C. Chen, R. Liu, and Z. Liu, “Ecg signal denoising based on multi-scale residual dense u-net,” in *Proceedings of the 2023 4th International Symposium on Artificial Intelligence for Medicine Science*, 2023, pp. 213–219.
- [53] J. Cheng, Y. Xu, R. Song, Y. Liu, C. Li, and X. Chen, “Prediction of arterial blood pressure waveforms from photoplethysmogram signals via fully convolutional neural networks,” *Computers in Biology and Medicine*, vol. 138, p. 104877, 2021.
- [54] R. A. Pinto, H. S. De Oliveira, E. Souto, R. Giusti, and R. Veras, “Inferring ecg waveforms from ppg signals with a modified u-net neural network,” *Sensors*, vol. 24, no. 18, p. 6046, 2024.
- [55] S. Bai, J. Z. Kolter, and V. Koltun, “An empirical evaluation of generic convolutional and recurrent networks for sequence modeling,” *arXiv preprint arXiv:1803.01271*, 2018.
- [56] J. PAN and W. J. TOMPKINS, “A real-time qrs detection algorithm,” *IEEE TRANSACTIONS ON BIOMEDICAL ENGINEERING*, vol. 32, no. 3, 1985.
- [57] D. B. Springer, L. Tarassenko, and G. D. Clifford, “Logistic regression-hmm-based heart sound segmentation,” *IEEE transactions on biomedical engineering*, vol. 63, no. 4, pp. 822–832, 2015.